Feasibility Study for Fused Deposition Modeling (FDM) 3D-Printed Propellers for Unmanned Aerial Vehicles

Lorenz R. Toleos, Jr., Niño Jhim Andrew B. Dela Luna, Mark Christian E. Manuel, John Marvil R. Chua, Eldric Marius A. Sangalang, and Patrick C. So
School of Mechanical and Manufacturing Engineering, Mapúa University, Manila, Philippines
Email: lrtoleos@gmail.com, {njabdelaluna, mcemanuel}@mapua.edu.ph, chua.john@hotmail.com, {sangalang.eldric, patrickcaringalso}@gmail.com

***Abstract*—Unmanned aerial vehicle (UAV) technology is being developed at a rapid pace, and its application can be seen on various fields and industry. One of the main challenges of UAVs is the limited energy, and majority of the power is consumed by the propulsion system. Thus, the efficiency and design of propellers is important to help increase the flight endurance. This study focuses on determining the feasibility of 3D-printed propellers for UAVs. The 3D printing technology utilized was the Fused Deposition Modeling (FDM), and the thermoplastic material used was a white Polylactic Acid (PLA). The propeller model that the researchers 3D-scanned is the APC Sport 9×6, which was fabricated at different 3D printer settings. The researchers developed a propeller testing apparatus and assessed the torque and thrust of the propellers using the said device. The impact strength of the propellers was also determined using a Charpy impact testing machine. Statistical treatments such as linear regression and T-test were utilized. The researchers found that FDM propellers have almost the same performance as the injection molded propeller at certain printer settings while other settings yielded an increase in torque. Since torque is directly proportional to the power consumption of the motor, it was determined that at certain printer settings, the FDM propellers consumes more power than injection molded propellers. Thus, the researchers were able to identify acceptable printer settings that can be used to 3D-print propellers. Also, the researchers found that the impact strength of FDM propellers is significantly lower than that of an injection molded propeller. With these findings, the researchers concluded that Fused Deposition Modelling can be used to verify the performance of new propeller designs before it goes into mass production, but because of the weaker mechanical strength, it is not optimal for actual use.**

***Index Terms*—unmanned aerial vehicles, propeller, 3D-printing, fused deposition modeling, performance analysis**

I. Introduction

Unmanned Aerial Vehicles (UAVs) are now part of our society and have developed at a rapid pace over the past few years [1] with the sales tripling to about $200 million [2]. UAVs were initially used and developed for military applications such as in World War I and II, Vietnam War, and Kuwait/Iraq War, among others [3], but as the technology develops and becomes more mainstream, commercial and civilian applications are becoming more common and essential [4]. Some of the applications of UAVs include aerial reconnaissance [5], [6], search and rescue operations [7], [8], risk and disaster management [9], [10], structural health inspections [11], [12], and resource monitoring and/or assessment [13]-[15]. UAVs also vary in size, from micro to large [3]. One of the most widely-used type of UAV is the quadrotor structure. Quadrotor-type UAVs are versatile, simple to build and assemble, and can take-off and land vertically [2]. A quadrotor UAV have four symmetrical arms, at the end of which are the motors, and the arms are connected to a central hub which houses the electronic components. Landing gears can also be installed at each arm. The hovering ability and easy maneuverability of quadrotor UAVs in 3-dimensional spaces prove to be a popular quality, as quadrotor UAVs are the most preferred type of UAVs for indoor and outdoor applications [4].

A typical quadrotor UAV is composed of four symmetrical arms, brushless DC electric motors at the end of each arm, propellers, electronic speed controllers, and a battery. The motor-driven propellers produce vertical thrust and thus generate the lift needed to move the vehicle upwards or downwards [2]. Batteries are the power source for motors, and most UAVs nowadays use Lithium-Polymer (Li-Po) batteries, which charge slowly but discharge fast [16]. The typical operation time of commercial UAVs is 20 minutes [17]. One of the challenges of UAVs is the limited energy and flight endurance [18] and about 85% of the power is consumed by the electric propulsion systems alone [19]. Structural resonance or vibration induced by the propellers is another drawback of quadrotor UAVs [4] and the aerodynamic performance of the UAVs are also dependent on the propellers [20]. As such, the design of propellers is very important for UAVs.

For an un-ducted rotor, the induced power (P) due to the lift is shown in (1), where L is the lift generated, ρ is the air density, and A is the area of the actuator disk [3].

Manuscript received March 15, 2019; revised March 10, 2020.

doi: 10.18178/ijmerr.9.4.548-558

$$P = L^{3/2} / (2\rho A)^{1/2} \qquad (1)$$

Several studies [21], [22], explored the design and manufacturing of propellers for small UAVs. Some manufacturing methods utilized were CNC milling, carbon fiber molds, and injection molding. Another manufacturing method that is currently gaining popularity is additive manufacturing or three-dimensional (3D) printing. The challenges and potential of additive manufacturing for Unmanned Aerial Vehicles were explored in [23] and [24]. Additive manufacturing has the capacity to produce moderate to mass quantities of products which reduces the manufacturing lead time and shortens the time of marketing new product designs or iterations. Some of the 3D printing technologies are Fused Deposition Modeling (FDM), Selective Laser Sintering (SLS), Stereolithography (SLA), and Digital Light Processing (DLP). Among these technologies, FDM is the most commonly used. In FDM 3D printers, thermoplastic materials are melted in the nozzle to produce the three-dimensional product based on a computer-aided design (CAD) file, which prints one layer at a time [25].

In this study, the researchers explored the feasibility of using FDM 3D printing technique in manufacturing propellers for unmanned aerial vehicles. The propeller model used for the study is the APC Sport 9×6 (9-inch diameter, 6-inch pitch) that rotates in the counter-clockwise direction. The propeller was 3D scanned and then manufactured in Tronxy X5S 3D printer using white Polylactic Acid (PLA) as the filament. The researchers designed and developed a propeller testing apparatus to measure the thrust and torque of the manufactured propellers. Charpy impact test was used to assess the mechanical strength of the propellers.

II. MATERIALS AND METHODS

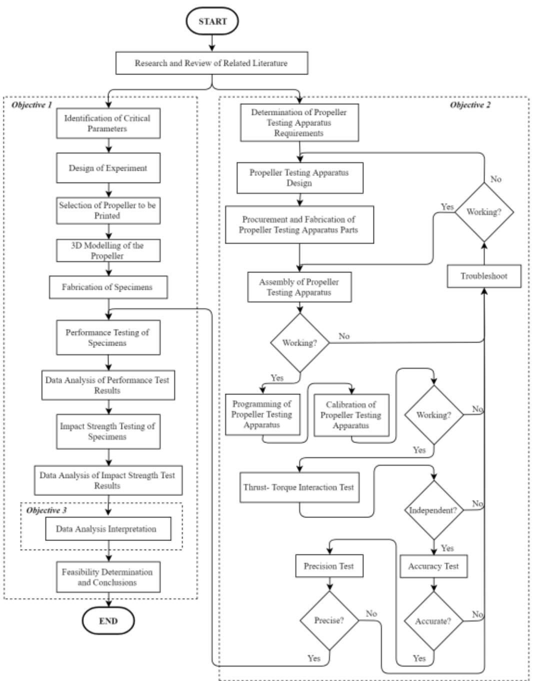

Figure 1. Methodological framework of the study.

The methodological framework for this study which shows the steps or processes that the researchers conducted to complete the research is shown in Fig. 1. The first phase of the study is the propeller selection, 3D scanning, and fabrication. The propeller was fabricated using an FDM 3D printer. There were eight printer setting combinations used, and each combination is printed twice to allow multiple trial testing. The phase 2 is the design and development of a propeller testing apparatus that can measure the thrust and torque of the mounted propeller at a given rotational speed. The third phase is the impact testing of the propellers using a Charpy impact testing device. The gathered data were then analyzed, and several statistical treatments were utilized such as linear regression, and T-test.

A. Propeller Selection, 3D Scanning, and Fabrication.

The APC Sport 9×6 (9-inch diameter, 6-inch pitch) that rotates in the counter-clockwise direction was selected because the study is only focused on 9-inch diameter propellers, and the propeller data of the APC Sport 9×6, which includes the geometry and performance, are available at the University of Illinois Urbana-Champaign (UIUC) propeller data site. The propeller manufacturer also published the performance data sheets (thrust and power consumption for different values of rpm) of the APC Sport 9×6.

The researchers availed the services of a local additive manufacturing company for the 3D scanning and modelling of the APC Sport 9×6 propeller, and the resulting stereolithography (STL) file is shown in Fig. 2.

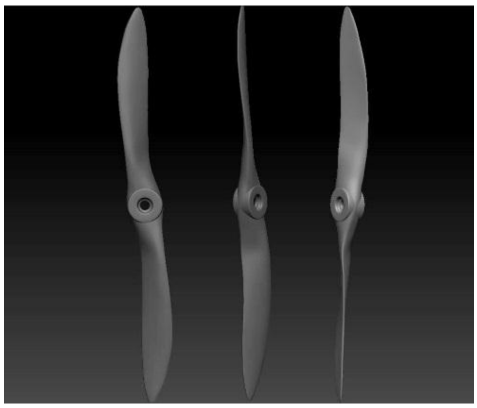

Figure 2. 3D model of the APC Sport 9×6.

The STL file was converted into G-Code using the slicer software Simplify 3D. The researchers fabricated 8 specimens with varying printer settings, which was selected in the Simplify 3D software. The parameters which were varied are the extruder temperature (°C), the printing speed (mm/min), and the layer height (mm). The extruder temperature is the temperature of the nozzle extrudes the filament. A high extruder temperature yields prints with high mechanical strength and low geometrical accuracy, while a low extruder temperature yields prints with low mechanical strength and high geometrical accuracy. Printing speed is the speed of the extruder's movement along the x and y axis. A high printing speed value results to a shorter printing time with less accurate print and low mechanical strength, while a low printing speed value results to a longer printing time with a more accurate print and high mechanical strength [26]. Layer height is the thickness of each printing layer along the z axis. A high layer height value results to a shorter printing time with less accurate print and low mechanical strength, while a low layer height value results to a longer printing time with a more accurate print and high mechanical strength [27]. Table I shows the specimen number corresponding to the combination of printer settings.

The specimens were fabricated using Tronxy X5S, an FDM 3D printer. The researchers used white PLA filament, as PLA is the most common filament used by FDM users, additionally, white was chosen because it is stronger than other colored PLA filaments due to the consistency of its crystalline structure [28]. Some of the 3D printed propellers are shown in Fig. 3.

TABLE I. SPECIMEN NUMBER CORRESPONDING TO THE COMBINATION OF PRINTER SETTINGS

Specimen No.	Extruder Temperature (°C)	Printing Speed (mm/min)	Layer Height (mm)
1	190	1800	0.10
2	190	1800	0.20
3	190	3600	0.10
4	190	3600	0.20
5	210	1800	0.10
6	210	1800	0.20
7	210	3600	0.10
8	210	3600	0.20

Figure 3. 3D model of the APC Sport 9×6.

B. Propeller Testing Apparatus

TABLE II. PROPELLER TESTING APPARATUS DESIGN REQUIREMENTS

Parameter	Value
Diameter	9 in
Maximum rotational speed	12000 rpm
Maximum thrust	1.57 kg_f
Maximum torque	0.150 N-m

The propeller testing apparatus was designed for a propeller with 9 inches of diameter. Some of the parameters such as the rotational speed and thrust were derived from a propeller survey by [29]. The propeller testing apparatus is able to measure the thrust and torque of the mounted propeller at a certain rotational speed. The parameters used for the propeller testing apparatus are shown in Table II.

One of the characteristics that classifies propellers is the aerodynamic power of the propeller or the power consumed by the propeller through the motors to rotate at a certain rotational speed. This characteristic is related to the drag force experienced by the propeller as it rotates around its axis. Like the thrust force, the drag force is also dependent on the airfoil distribution of the propeller and on the angle of attack of the airfoil cross sections, additionally, drag is also related to the length of span of the propeller which results in vortices that makes induced drag, this implies that propellers with different designs will have different aerodynamic power vs rpm distributions [30]. Instrumentations wise, the power required by the propeller to rotate at a certain rpm cannot be measured directly, it needs to be computed from values measured using sensors. The sensors are able to determine the torque and the rpm of the motor connected to the propeller at a given time. Because the motor is directly coupled to the propeller, the power produced by this motor through the output shaft goes directly to the propeller, it can be assumed that the transmission losses of this setup is negligible because the shafting from the motor to the propeller is small. Thus, it can be assumed that the shaft power is also equal to the aerodynamic power. The relationship between the aerodynamic power, torque, and rotational speed is given by (2), where P is the aerodynamic power (W), T is the torque (N-m), and n is the rotational speed (rpm).

$$P = Tn\,(2\pi / 60) \qquad (2)$$

Figure 4. Main body of the propeller testing apparatus.

The propeller testing apparatus is composed of a motor, electronic speed controller (ESC), power supply, microcontroller, thrust sensor, torque sensor, rotational speed sensor, rotational speed controller, and an input keypad and a liquid crystal display (LCD) as the graphical user interface (GUI). The components of the apparatus were installed on a 3D printed body. An acrylic shield was also installed which served as protections for users and ducting on the apparatus to maximize airflow. The distance between the propeller tips and the acrylic shield is 2 inches. The main body of the apparatus is shown in Fig. 4.

The propeller testing apparatus calibrated using a Hall effect sensor, wherein the optimal distance of the Hall sensor from the magnet and the optimal elapsed time were determined. The 3D printed specimens were each tested in the propeller testing apparatus to determine the respective torque and thrust of the specimens.

1) Thrust

Thrust are generated by propellers and the generation of such force can be attributed to the principles of Bernoulli. With the increase in velocity over a curved surface, the air pressure on that surface is then lowered, which then pulls the propeller. Furthermore, the fundamental principle in generating thrust and lift is the momentum change of the mass of air which moves into the propeller disk. In the case of quadrotor-type UAVs, the momentum generator is the rotor which produces the most efficient powered lift for hovering in comparison with other momentum generators. Rotors have large disk area which translates to the movement of large mass of air at low velocity. The relationship between the lift (L), power (P), and exit velocity (V_e) is shown in (3). Equation (3) shows that the lift per unit power have an inversely proportional relationship with exit velocity [3].

$$L / P = 2 / V_e \tag{3}$$

UAVs can be moved forwards or backwards by tilting the rotor's plane of rotation which then converts some net aerodynamic force into thrust. In order to maintain the lift needed to carry the aircraft, the total aerodynamic force needs to be increased which is achieved by inputting more power to the rotors [3].The thrust produced by a propeller depends on the airfoil cross section distribution of the propeller and the angle of attack. Propellers with different designs will have different thrust vs rpm distributions. Varying the pitch of the propeller while maintaining a constant diameter dramatically changes the thrust produced by the propeller at a certain rpm [30].

2) Torque

Based on the principles of Newton's third law of motion which focuses on action and reaction, an aircraft tends to rotate in the opposite direction of the rotation of the rotor blades, and this phenomenon is called torque. Torque must be counteracted before the aircraft can fly and one way of counteracting the torque is by using dual or multiple rotors [31]. The torque (T) produced by an electric motor is given in (4).

$$T = K_t(I - I_n) \tag{4}$$

In (4), K_t is the torque constant of the motor, I is the current which produces torque, and I_n is the no-load current. The torque constant of the motor is also a measure of the motor's efficiency and is usually given by the manufacturer. Equation (3) shows that the torque (T) is proportional to the current (I) passing through the motor's coils [3].

The efficiency of the propeller and the rotor have a proportional relationship with the area of the actuator disk, which is proportional to the square of the diameter of the propeller. Additionally, the efficiency in producing thrust or lift is at its maximum when the disk diameter is large, and the rotational speed is slow. When using electric motors, the value of torque can remain constant at any rpm. However, in order to lessen the weight and size of the motor, the motor can first be run at high rotational speed and then gear it down as needed, in accordance to the required propeller diameter, rotor torque, and rpm [3].

C. Charpy Impact Test.

Charpy impact testing have been utilized to estimate different mechanical properties using elevated loads [32]. In a Charpy impact test, a heavy pendulum is swung through a material. The difference in initial and final height of the pendulum is then measured, this difference is then used to calculate for the energy lost (and therefore work done) of the pendulum. The Charpy impact testing apparatus in the Materials Testing Laboratory of Mapúa University was utilized to test the impact strength of the printed specimens. The commercially-available APC Sport 9×6 was also tested for its impact strength, and the results were compared with that of the specimens. The propellers were cut into two parts because the test was conducted on the propeller blades and not on the central hub. The Charpy impact testing apparatus and a specimen loaded in the apparatus are shown in Fig. 5.

Figure 5. Charpy impact testing apparatus (a) and a propeller specimen loaded in the testing device (b).

D. Statistical Treatment

Linear regression is the use of polynomials to estimate the response of an event using the data gathered. Polynomial linear regression was utilized by the researchers and 2nd order polynomial (quadratic) equations were created for the gathered data. The coefficient of determination (R^2), which is the measure of the suitability of the regression model, was also computed for each of the polynomial linear regressions. A high coefficient of determination tells the analyst that the regression model represents the data accurately, this parameter was used in this research as the researchers constructed a line of best fit for the data the researchers had gathered that they used for interpolation of values. Because a higher order polynomial would always tend the R^2 to unity (more terms would provide more curves/inflection points to the regression line allowing closer estimation but this does not mean that the regression line is conceptually correct), an adjusted coefficient of determination was utilized, this is R^2_{adj}, which better describes if the regression line models the data correctly.

The T-test was used to analyze the difference in means between two data sets of different populations. In this research, this is the hypothesis testing utilized by the researchers to determine if the performance of the specimen propellers is the same as the performance of the original propeller. In this case, the performance of the specimen propellers was visualized as a sample from the population with a certain central value or mean. The performance of the control propeller was also determined. The two propellers can be said to have similar performance if their means is the same. Thus, it can be surmised that if the value of the means of a specimen propeller is nearly the same of the original controller, they will also have very similar performance.

III. Results and Discussion

A. *Propeller Performance Test*

The thrust and torque of eight specimens were measured at ten rotational speeds from about 2,000 to 8,000. For each specimen combination and each rotational speed, three trials were tested to determine the mean, the first and second trials were from a first print of a certain specimen, and the third trial is from a reprint of that specimen. Similarly, five trials for 10 rotational speeds were conducted for the original propeller to determine the mean values. The rotational speed or rpm of the motor was controlled using a Digital Servo Tester ESC Consistency Tester to send the Pulse Width Modulation (PWM) signal to the ESC. Since even entering the same input value for the PWM yields a different rpm for each trial, the ten rpm per specimen trial were gathered so that a line of best fit for each trial can be calculated. From the line of best fit, a quadratic equation was derived, and the corresponding parameters were interpolated at fixed rpm, from 2400 rpm to 7500 rpm, at 300 rpm intervals, resulting into eighteen rotational speeds and their corresponding data sets.

1) *Thrust*

A thrust load cell was used as the thrust sensor of the propeller testing apparatus. The maximum thrust is set at 1.57 kg_f and the nearest load cell that can measure this load is a 3 kg_f Straight Bar Load Cell, thus it was the load cell used by the researchers. A load cell amplifier was also used to raise the voltage reading of the load cell to a voltage level recognizable by the microcontroller. For this, the researchers used Load Cell Amplifier HX711. The thrust sensor was able to record the thrust at a given rpm, but since the rpm reading is not constant, ten thrust readings were first recorded for each trial, and the equation was derived to compare the data sets of each specimens at similar rpms. The raw data for the thrust measurements (at 10 rotational speeds) were graphed, and a 2nd degree polynomial linear regression was created to determine the corresponding quadratic equations and coefficient of determination (R^2) of the various trials of the different specimens and of the original specimen. The quadratic equation was used to determine the approximate thrust measurements of each specimens at certain rotational speeds (18 rotational speeds, from 2400 rpm to 7500 rpm, with 300 rpm interval). The graph of the raw thrust readings of the specimens as compared to the original is shown in Fig. 6. Table III shows the interpolated thrust readings of each specimens at eighteen different rotational speeds. The thrust values in Table III are the average thrust measurements of the different trials of each specimen propeller.

2) *Torque*

Two torque load cells were used as the torque sensor of the propeller testing apparatus. The load cells were set into a couple configuration having a known distance from the center of rotation of the motor. This allows the apparatus to measure the torque by multiplying the force read by the load cells to the distance between the two load cells. From the width of the motor, the researchers used a distance of 2 in, with a maximum couple moment of 0.150 N-m as stated. The maximum force was calculated to be 3.94 N, which corresponds to 0.301 kg_f. The nearest load cell that can measure this force is a 1 kg_f Straight Bar Load Cell. Like the set-up of the thrust instrumentation, the torque load cells also need an amplifier to work. The same Load Cell Amplifier HX711 was used by the researchers for each torque load cell. Because the couple principle was used in the torque measurement, two load cells and two amplifiers were required to measure the couple force correctly. The torque sensor was able to record the thrust at a given rpm, but since the rpm reading is not constant, ten thrust readings were first recorded for each trial, and the equation was derived to compare the data sets of each specimens at similar rpms. The raw data for the torque measurements (at 10 rotational speeds) were graphed, and a 2nd degree polynomial linear regression was created to determine the corresponding quadratic equations and coefficient of determination (R^2) of the various trials of the different specimens and of the original specimen. The quadratic equation was used to determine the approximate torque measurements of each specimens at certain rotational speeds (18 rotational speeds, from 2400 rpm to 7500 rpm, with 300 rpm interval). The graph of the raw torque readings of the specimens as compared to the original is shown in Fig. 7. Table IV shows the interpolated torque readings of each specimens at eighteen different rotational speeds. The torque values in Table IV are the average torque measurements of the different trials of each specimen propeller.

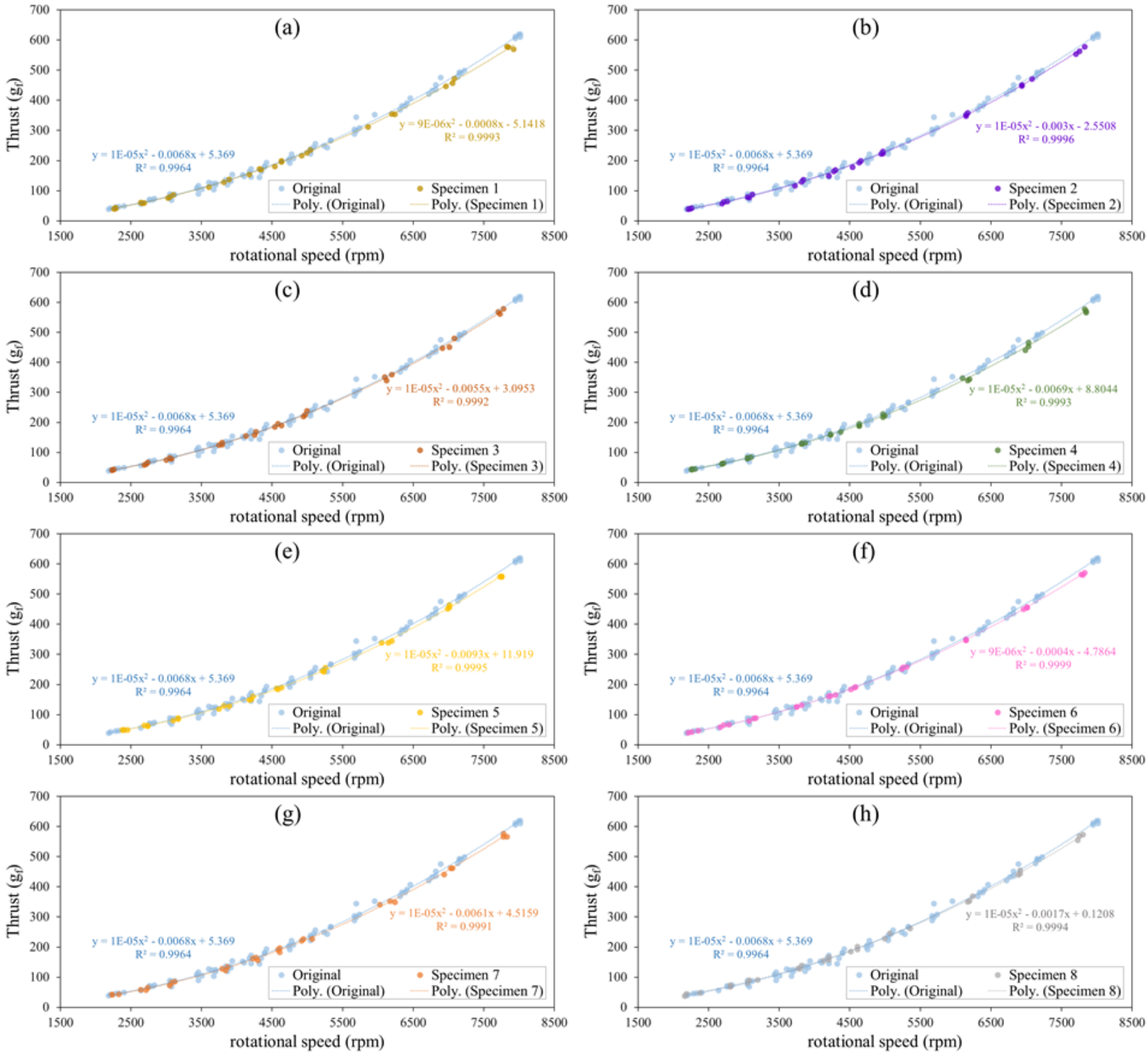

Figure 6. Thrust readings of propeller specimens: specimen 1 (a), specimen 2 (b), specimen 3 (c), specimen 4 (d), specimen 5 (e), specimen 6 (f), specimen 7 (g), specimen 8 (h); as compare to the thrust readings for the original propeller.

TABLE III. AVERAGED THRUST READINGS FOR EACH SPECIMEN IN GRAM-FORCE

Rotational Speed (RPM)	Original	Specimen 1	Specimen 2	Specimen 3	Specimen 4	Specimen 5	Specimen 6	Specimen 7	Specimen 8
2400	48.99	47.69	47.00	48.34	49.94	49.14	48.68	47.89	51.34
2700	62.98	61.90	61.13	62.24	63.21	62.16	63.00	61.48	65.53
3000	78.84	77.83	77.03	77.97	78.29	77.05	79.02	76.89	81.46
3300	96.57	95.47	94.70	95.53	95.18	93.80	96.74	94.12	99.11
3600	116.16	114.82	114.15	114.91	113.87	112.42	116.17	113.17	118.49
3900	137.62	135.88	135.37	136.13	134.37	132.90	137.30	134.03	139.60
4200	160.94	158.66	158.37	159.17	156.67	155.25	160.13	156.71	162.45
4500	186.13	183.14	183.13	184.04	180.79	179.46	184.66	181.20	187.01
4800	213.18	209.34	209.67	210.74	206.71	205.53	210.89	207.52	213.31
5100	242.10	237.26	237.99	239.27	234.43	233.47	238.83	235.65	241.34
5400	272.89	266.88	268.07	269.63	263.97	263.27	268.47	265.59	271.10
5700	305.54	298.22	299.93	301.81	295.31	294.93	299.81	297.36	302.59
6000	340.06	331.27	333.56	335.83	328.46	328.46	332.85	330.94	335.80
6300	376.44	366.04	368.97	371.67	363.41	363.86	367.60	366.33	370.75
6600	414.69	402.51	406.15	409.34	400.17	401.11	404.05	403.55	407.42
6900	454.80	440.70	445.10	448.84	438.74	440.24	442.19	442.58	445.82
7200	496.78	480.60	485.82	490.17	479.11	481.22	482.05	483.42	485.96
7500	540.63	522.21	528.32	533.33	521.30	524.07	523.60	526.09	527.82

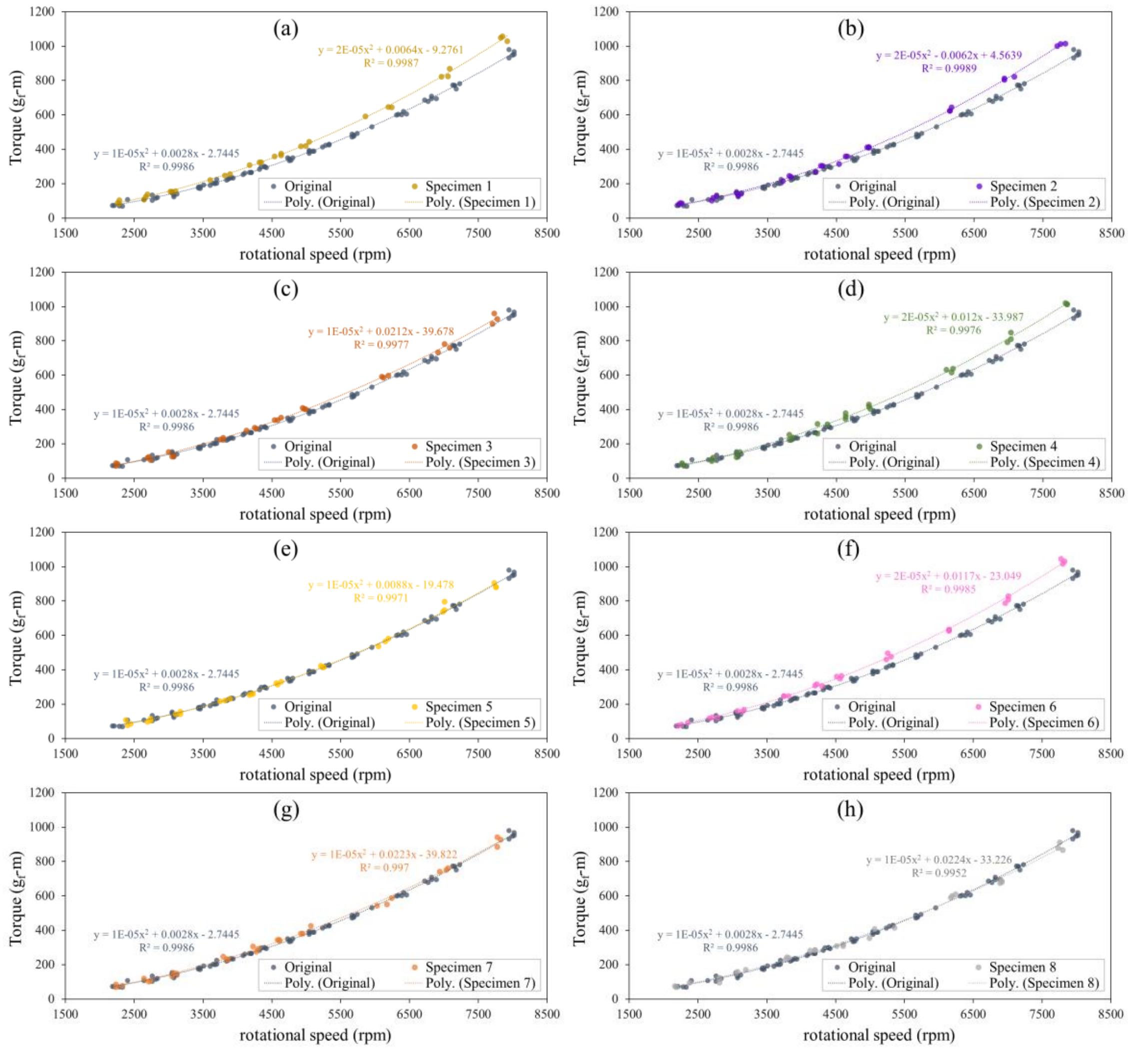

Figure 7. Torque readings of propeller specimens: specimen 1 (a), specimen 2 (b), specimen 3 (c), specimen 4 (d), specimen 5 (e), specimen 6 (f), specimen 7 (g), specimen 8 (h); as compare to the torque readings for the original propeller.

TABLE IV. AVERAGED TORQUE READINGS FOR EACH SPECIMEN IN GRAM-FORCE-MASS

Rotational Speed (RPM)	Original	Specimen 1	Specimen 2	Specimen 3	Specimen 4	Specimen 5	Specimen 6	Specimen 7	Specimen 8
2400	88.45	99.67	90.92	88.19	84.50	83.43	95.27	87.37	91.11
2700	111.67	126.34	115.70	115.08	111.96	107.88	122.71	113.81	116.52
3000	137.54	155.94	143.64	144.37	142.22	134.89	152.97	142.56	144.13
3300	166.06	188.48	174.76	176.08	175.29	164.46	186.04	173.61	173.96
3600	197.22	223.95	209.04	210.19	211.15	196.59	221.93	206.97	205.99
3900	231.04	262.37	246.50	246.71	249.82	231.28	260.63	242.64	240.23
4200	267.50	303.72	287.12	285.65	291.29	268.53	302.15	280.60	276.68
4500	306.61	348.00	330.92	326.99	335.56	308.35	346.49	320.88	315.34
4800	348.38	395.22	377.88	370.74	382.63	350.72	393.64	363.46	356.21
5100	392.79	445.38	428.02	416.91	432.51	395.66	443.60	408.34	399.29
5400	439.85	498.48	481.33	465.48	485.19	443.16	496.38	455.53	444.58
5700	489.56	554.51	537.80	516.46	540.67	493.21	551.98	505.03	492.08
6000	541.92	613.48	597.45	569.85	598.95	545.83	610.39	556.83	541.79
6300	596.93	675.39	660.27	625.66	660.04	601.02	671.61	610.94	593.70
6600	654.58	740.23	726.26	683.87	723.93	658.76	735.65	667.35	647.83
6900	714.89	808.01	795.42	744.49	790.62	719.06	802.51	726.07	704.16
7200	777.85	878.72	867.75	807.52	860.11	781.93	872.18	787.09	762.70
7500	843.45	952.38	943.25	872.96	932.41	847.35	944.67	850.42	823.46

B. Propeller Impact Strength Test

The impact strength of the propellers were measured using the Charpy impact testing device. The previous performance test was done to determine if the performance of the 3D printed propeller is similar to the performance of the control propeller. This is the first step in determining if 3D printing can be used to manufacture UAV propellers. The results from the previous test will determine if the performance is similar and because of such will signify that 3D printing the propeller can be used as a design verification step to approximate the performance of a newly designed propeller by 3D printing it and testing it in a propeller testing apparatus. The next step in determining if 3D printing can be used to manufacture UAV propellers is by testing its mechanical strength and comparing it to the off-the-shelf propeller. This step determines if the 3D printed propeller is safe to be flown and can be used in real applications outside the laboratory setting.

Figure 8. Sawed specimens for impact testing.

As the propeller will fail by colliding with an obstacle while it is rotating, impact strength testing was utilized by the researchers. Other researchers employed tensile testing of the propeller, but the researchers believe that the results from tensile testing does not relate to the "air worthiness" of the propeller because in application, the loads carried by the propeller is not only tensile in nature. In application, combined tensile (from centrifugal force) and multi-axis bending (from lift and drag produced by each airfoil cross section) is carried by the propeller, thus, because 3D printing parts are inherently anisotropic, tensile testing it would not tell anything to its mechanical performance while in use. Lastly, the propeller's cross section is not aligned and consistent thus, using tensile test does not ensure that the load bore by the propeller is purely tensile, there would be stress concentrations and points of bending because of non-uniform flow of stress. To prepare the specimens, it was first sawed apart so that it can be loaded to the apparatus as shown in Fig. 8. Next, the specimen was loaded in the apparatus. As the researchers are interested on the impact strength of the propeller while in use, a standard specimen for Charpy Impact Testing was not utilized. The propeller was loaded as is. To avoid variation in the results, the propellers were loaded similarly throughout all the tests.

The impact strength of the specimen propellers for four trials each combination, is shown in Table V. The similarity is calculated by simple comparison of means, because the mean value is significantly far from each other, the researchers did not utilize any statistical analysis technique for the comparison. The values in this table shows that the 3D printed propellers are significantly weaker than the injection molded propeller.

The researchers also tested the impact strength of a horizontally-printed propeller to determine if a change in printing orientation would result in a more favorable impact strength that is closer to the original propeller. The result of this test is shown in Table VI, which shows that the impact strength of the 3D-printed propeller in horizontal orientation is almost double than that of the specimen propellers (which has vertical orientation) but is still significantly lower than that of the injection molded (original) propeller.

C. T-Test for Thrust and Torque

Using the data from Table III and Table IV, T-test equivalence between two population means were created as the thrust and torque readings are all at the same rpm levels and the null hypothesis is shown in Table VII.

TABLE V. Impact Strength (N-m) of Specimens and Original Propeller

Sample	Trial 1	Trial 2	Trial 3	Trial 4	Mean
1	0.40	0.30	0.40	0.30	0.35
2	0.35	0.35	0.40	0.40	0.38
3	0.25	0.30	0.30	0.35	0.30
4	0.40	0.30	0.30	0.25	0.31
5	0.45	0.40	0.50	0.50	0.46
6	0.50	0.45	0.40	0.45	0.45
7	0.40	0.40	0.50	0.40	0.43
8	0.60	0.40	0.45	0.40	0.46
Original	6.00	5.30	-	-	5.65

TABLE VI. Impact Strength (N-m) of Propeller Printed in Horizontal Direction

Sample	Trial 1	Trial 2	Mean
Horizontally-printed	0.75	1.25	1
Vertically-printed (mean)	-	-	0.39
Original	6.00	5.30	5.65

TABLE VII. Impact Strength (N-m) of Specimens and Original Propeller

Difference in Means Hypothesis Test (Two-tailed T-test) (α=0.05)	
Null Hypothesis	H_0: $\mu_{specimen} - \mu_{control} = 0$
Alternative Hypothesis	H_a: $\mu_{specimen} - \mu_{control} \neq 0$

TABLE VIII. T-TEST RESULTS FOR THRUST OF SPECIMEN 1

RPM	Xo-Xs	Stdev	v	t	P-value	Conclusion
2400	1.30	1.96	5	0.66	0.54	NOT REJECT
2700	1.08	2.29	5	0.47	0.66	NOT REJECT
3000	1.02	3.01	5	0.34	0.75	NOT REJECT
3300	1.10	3.79	5	0.29	0.78	NOT REJECT
3600	1.34	4.49	5	0.30	0.78	NOT REJECT
3900	1.74	5.10	5	0.34	0.75	NOT REJECT
4200	2.28	5.58	5	0.41	0.70	NOT REJECT
4500	2.98	5.94	5	0.50	0.64	NOT REJECT
4800	3.84	6.18	5	0.62	0.56	NOT REJECT
5100	4.84	6.29	5	0.77	0.48	NOT REJECT
5400	6.00	6.29	5	0.95	0.38	NOT REJECT
5700	7.32	6.19	5	1.18	0.29	NOT REJECT
6000	8.78	6.01	5	1.46	0.20	NOT REJECT
6300	10.40	5.77	5	1.80	0.13	NOT REJECT
6600	12.18	5.53	5	2.20	0.08	NOT REJECT
6900	14.10	5.35	5	2.64	0.05	REJECT
7200	16.18	5.32	4	3.04	0.04	REJECT
7500	18.42	5.52	2	3.34	0.08	NOT REJECT

An example of a T-test for a printed specimen is shown in Table VIII. In this type of test, rejecting the null hypothesis would mean that the alternative hypothesis is strongly supported by the data. Thus, if the null hypothesis is rejected at a certain level of rpm, the data supports that the thrust produced by the control propeller and the specimen propeller at the specified rpm is not equal. The proportion of the non-rejected rpm levels was then calculated by the researchers to compare the different specimens. It is important to note that the fixed rpm levels should be inside the rpm range where all the propellers were measured, which ensures that the thrust and torque values are interpolations not extrapolations. This criterion influenced the levels of rpm that were interpolated.

From Table VIII, the researchers calculated the proportion p to be $p = 16/18 = 0.89$, this was used by the researchers to compare specimen propeller types to each other. This means that 89% of the thrust readings from (2400 rpm to 7500 rpm) of the specimens are the same with that of the original propeller.

The T-test results table for the torque readings of specimen 1 is shown in Table IX. The proportion for the torque readings of this specimen 1 is calculated to be $p = 2/18 = 0.11$, this can be interpreted as for 11% of the range of the rpm readings from 2400 rpm to 7500 rpm, the torque produced from the specimen propeller is the same as the torque produced from the original control propeller, this interpretation is supported by the nature of the statistical test used.

TABLE IX. T-TEST RESULTS FOR TORQUE OF SPECIMEN 1

RPM	Xo-Xs	Stdev	v	t	P-value	Conclusion
2400	-11.22	7.77	5	-1.44	0.21	NOT REJECT
2700	-14.67	6.26	5	-2.34	0.07	NOT REJECT
3000	-18.40	4.85	5	-3.79	0.01	REJECT
3300	-22.42	3.59	5	-6.25	0.00	REJECT
3600	-26.73	2.56	5	-10.44	0.00	REJECT
3900	-31.33	2.02	5	-15.49	0.00	REJECT
4200	-36.22	2.25	5	-16.13	0.00	REJECT
4500	-41.39	3.01	3	-13.75	0.00	REJECT
4800	-46.85	3.98	3	-11.76	0.00	REJECT
5100	-52.59	5.03	3	-10.46	0.00	REJECT
5400	-58.63	6.10	3	-9.61	0.00	REJECT
5700	-64.95	7.18	2	-9.04	0.01	REJECT
6000	-71.56	8.28	2	-8.65	0.01	REJECT
6300	-78.46	9.38	2	-8.36	0.01	REJECT
6600	-85.64	10.51	2	-8.15	0.02	REJECT
6900	-93.12	11.67	2	-7.98	0.02	REJECT
7200	-100.88	12.86	2	-7.85	0.02	REJECT
7500	-108.93	14.09	2	-7.73	0.02	REJECT

TABLE X. PROPORTION OF "NOT REJECTED" RPM LEVELS TO THE TOTAL RPM LEVELS FOR ALL SPECIMEN TYPES

Specimen	Thrust	Torque	Conclusion
1	0.89	0.11	REJECTED
2	0.89	0.33	REJECTED
3	1.00	0.33	REJECTED
4	1.00	0.56	REJECTED
5	0.78	1.00	NOT REJECTED
6	0.83	0.11	REJECTED
7	0.89	0.83	NOT REJECTED
8	0.94	0.72	NOT REJECTED

The visual interpretation of the T-test result can be seen in Fig. 6 and Fig. 7, in these figures, the readings from the specimen propellers were plotted with the readings from the original propeller. As shown, a high proportion indicates that the readings from the specimen propeller lies around the readings of the original propeller while a low proportion indicates that the readings from the specimen propeller is far from the readings of the original propeller. The tabulated compilation of the proportion p values for all the propeller specimens is shown in Table X.

The values with $p < 0.7$ were highlighted with yellow in Table X. As shown in the table, only three specimens were within acceptable proportions for the torque readings. Analyzing the data used for these calculations, it is evident that the torque readings produced by the specimen propellers are typically higher than the torque produced by the original propeller. This signifies that the power consumption of 3D-printed propellers is higher than that of the original injection-molded propeller. The table also shows that for the thrust readings, the proportion is not affected too much by varying the printer settings as compared to the variation seen in the torque.

IV. CONCLUSIONS AND RECOMMENDATIONS

A. *Conclusions*

After the completion of the activities discussed in this paper along with the data analysis and interpretation, the researchers can conclude that this study was able to determine the feasibility of using Fused Deposition Modeling to manufacture propellers for Unmanned Aerial Vehicles by determining if the performance and the mechanical strength of the 3D printed propellers is the same as the injection molded propellers.

The objectives were achieved using the performance test and impact strength test discussed in the previous sections of this study. The researchers were able to find that FDM 3D-printing is not feasible to be used in manufacturing drone propellers because of its significantly weaker impact strength, but it can be used to approximate the performance of the injection-molded propeller especially as a design verification process because the performance of the 3D-printed propellers fabricated using specific printer settings (specimens 5, 7, and 8) have similar performance with the original injection-molded propeller.

B. Recommendations

For researchers wanting to explore the feasibility of using 3D-printing to manufacture propellers, the researchers recommend that the future researchers use other 3D-printing techniques and other 3D-printing materials as the researchers had found that using FDM 3D-printing to manufacture propellers is not optimal for actual use because of the low impact strength the 3D-printed propellers produce. Other 3D-printing techniques like Stereolithography (SLA) might be better suited for this application as SLA 3D-printed specimens might have higher impact strength. Other filaments like polypropylene, ABS, and others could also be the focus of future researchers as this might yield different results in mechanical strength

The researchers also recommend studying in-depth, the field of probability and statistic. The researchers believe that knowledge from this field should be standard to everyone doing research as knowledge in probability and statistics would provide a strong footing in the field of research, where strong conclusions can be drawn using statistical methods or analysis. Other statistical treatment can also be applied to the data of the future researchers such as the analysis of variance (ANOVA) among others.

CONFLICT OF INTEREST

There is no conflict of interest for this study.

AUTHOR CONTRIBUTIONS

Lorenz R. Toleos, John Marvil R. Chua, Eldric Marius A. Sangalang, and Patrick C. So developed the prototype and conducted the study. Mark Christian E. Manuel and Niño Jhim Andrew B. Dela Luna supervised ang guided the study, especially the paper writing.

ACKNOWLEDGMENT

The authors would like to express their gratitude to the Commission on Higher Education (CHED) of the Philippines which has funded this research project through its DARE-TO (Discovery-Applied Research and Extension for Trans/Inter-disciplinary Opportunities) research grant for the project: "Unmanned Aerial Monitoring and Information Management of Aging Structures". The authors would also like to thank Mapúa University for providing the facilities which made this study possible.

REFERENCES

[1] Y. Li, H. Lu, Y. Nakayama, H. Kim, and S. Serikawa, "Automatic road detection system for an air–land amphibious car drone," *Future Generation Computer Systems*, vol. 85, pp. 51-59, March 2018.

[2] A. Martinetti, M. Margaryan, and L. van Dongen, "Simulating mechanical stress on a micro Unmanned Aerial Vehicle (UAV) body frame for selecting maintenance actions," *Procedia Manufacturing*, vol. 16, pp. 61-66, 2018.

[3] P. G. Fahlstrom and T. Gleason, *Introduction to UAV systems*, 4th ed. Chichester, U.K.: Wiley, 2012.

[4] A. Tullu, Y. Byun, J. N. Kim, and B. S. Kang, "Parameter optimization to avoid propeller-induced structural resonance of quadrotor type Unmanned Aerial Vehicle," *Composite Structures*, vol. 193, pp. 63-72, June 2018.

[5] Z. Wang, L. Liu, T. Long, and Y. Wen, "Multi-UAV reconnaissance task allocation for heterogeneous targets using an opposition-based genetic algorithm with double-chromosome encoding," *Chinese Journal of Aeronautics*, vol. 31, no. 2, pp. 339-350, February 2018.

[6] B. H. Sheu, C. C. Chiu, W. T. Lu, C. C. Lien, T. K. Liu, and W. P. Chen, "Dual-axis rotary platform with UAV image recognition and tracking," *Microelectronics Reliability*, vol. 95, pp. 8-17, April 2019.

[7] M. Półka, S. Ptak, and Ł. Kuziora, "The use of UAV's for search and rescue operations," *Procedia engineering*, vol. 192, pp. 748-752, 2017.

[8] E. Lygouras, A. Gasteratos, K. Tarchanidis, and A. Mitropoulos, "ROLFER: A fully autonomous aerial rescue support system," *Microprocessors and Microsystems*, vol. 61, pp. 32-42, May 2018,.

[9] M. Erdelj, M. Król, and E. Natalizio, "Wireless sensor networks and multi-UAV systems for natural disaster management," *Computer Networks*, vol. 124, pp. 72-86, September 2017.

[10] P. D. Bravo-Mosquera, L. Botero-Bolivar, D. Acevedo-Giraldo, and H. D. Cerón-Muñoz, "Aerodynamic design analysis of a UAV for superficial research of volcanic environments," *Aerospace Science and Technology*, vol. 70, pp. 600-614, November 2017.

[11] S. Sankarasrinivasan, E. Balasubramanian, K. Karthik, U. Chandrasekar, and R. Gupta, "Health monitoring of civil structures with integrated UAV and image processing system," *Procedia Computer Science*, vol. 54, pp. 508-515, 2015.

[12] W. K. Chiu, W. H. Ong, T. Kuen, and F. Courtney, "Large structures monitoring using unmanned aerial vehicles," *Procedia Engineering*, vol. 188, pp. 415-423, 2017.

[13] J. Senthilnath, M. Kandukuri, A. Dokania, and K. N. Ramesh, "Application of UAV imaging platform for vegetation analysis based on spectral-spatial methods," *Computers and Electronics in Agriculture*, vol. 140, pp. 8-24, August 2017.

[14] S. Baena, D. S. Boyd, and J. Moat, "UAVs in pursuit of plant conservation – Real world experiences," *Ecological Informatics*, vol. 42, pp. 2-9, September 2018.

[15] R. Woellner and T. C. Wagner, "Saving species, time and money: Application of unmanned aerial vehicles (UAVs) for monitoring of an endangered alpine river specialist in a small nature reserve," *Biological Conservation*, vol. 233, pp. 162-175, May 2019.

[16] P. G. Sai, C. S. Rani, and U. R. Nelakuditi, "Implementation of power optimization technique for UAVs," *Materials Today: Proceedings*, vol. 5, no. 1, pp. 132-137, 2018.

[17] Y. Li, H. Lu, Y. Nakayama, H. Kim, and S. Serikawa, "Automatic road detection system for an air–land amphibious car drone," *Future Generation Computer Systems*, vol. 85, pp. 51-59, March 2018.

[18] D. C. Gandolfo, L. R. Salinas, M. E. Serrano, and J. M. Toibero, "Energy evaluation of low-level control in UAVs powered by lithium polymer battery," *ISA Transactions*, vol. 71, pp. 563-572, November 2017.

[19] R. Schacht-Rodríguez, J. C. Ponsart, C. D. García-Beltrán, and C. M. Astorga-Zaragoza, "Prognosis & health management for the prediction of UAV flight endurance," *IFAC-PapersOnLine*, vol. 51, no. 24, pp. 983-990, 2018.
[20] K. Wang, Z. Zhou, X. Zhu, and X. Xu, "Aerodynamic design of multi-propeller/wing integration at low Reynolds numbers," *Aerospace Science and Technology*, vol. 84, pp.1-17, 2019.
[21] I. P. Tracy, "Propeller design and analysis for a small, autonomous UAV," Ph.D. dissertation, Massachusetts Institute of Technology, Cambridge, MA, 2011.
[22] J. Stockton, B. Bettinger, A. Arena, R. Gaeta, and J. Jacob, "Design and Manufacturing of Composite Propellers for SUAS," in *51st AIAA Aerospace Sciences Meeting including the New Horizons Forum and Aerospace Exposition*, 2013, p. 498.
[23] C. Ferro, R. Grassi, C. Seclì, and P. Maggiore, "Additive manufacturing offers new opportunities in UAV research," *Procedia CIRP*, vol. 41, pp. 1004-1010, 2016.
[24] G. D. Goh, S. Agarwala, G. L. Goh, V. Dikshit, S. L. Sing, and W. Y. Yeong, "Additive manufacturing in unmanned aerial vehicles (UAVs): Challenges and potential," *Aerospace Science and Technology*, vol. 63, pp. 140-151, 2017.
[25] M. Attaran, "The rise of 3-D printing: The advantages of additive manufacturing over traditional manufacturing," *Business Horizons*, vol. 60, no. 5 pp. 677-688, 2017.
[26] F. Johansson, "Optimizing Fused Filament Fabrication 3D printing for durability: Tensile properties and layer bonding," M.S. thesis, Dept. Mech. Eng., Blekinge Institute of Technology, 2016.
[27] G. S. Bual, and P. Kumar, "Methods to improve surface finish of parts produced by fused deposition modeling," *Manufacturing Science and Technology*, vol. 2, no. 3, pp. 51-55, 2014.
[28] B. Wittbrodt and J. M. Pearce, "The effects of PLA color on material properties of 3-D printed components," *Additive Manufacturing*, vol. 8, pp. 110-116, October 2015.
[29] M. M. Borges, "Design of an Apparatus for Wind Tunnel Tests of Electric UAV Propulsion Systems," M.S. thesis, Instituto Superior Técnico, Universidade de Lisboa, Portugal, 2015.
[30] R. W. Deters, G. K. Ananda, and M. S. Selig, "Reynolds number effects on the performance of small-scale propellers," in *32nd AIAA applied aerodynamics conference*, p. 2151, 2014.
[31] C. E. Dole, J. E. Lewis, J. R. Badick, and B. A. Johnson, *Flight Theory and Aerodynamics: A Practical Guide for Operational Safety*, 3rd ed. New Jersey: John Wiley & Sons, 2017, ch. 17, pp. 326-327.
[32] E. Lucon, "Estimating dynamic ultimate tensile strength from instrumented Charpy data," *Materials & Design*, vol. 97, pp. 437-443, 2016, doi:10.1016/j.matdes.2016.02.116.

Lorenz R. Toleos, Jr. is an undergraduate student of Bachelor of Science in Mechanical Engineering in Mapúa University.
He is currently a Science Research Assistant for a CHED – DARE TO research project in the research building of Mapúa University. His research interests include instrumentations, robotics, and rapid prototyping.

Niño Jhim Andrew B. Dela Luna was born in January 29, 1995. He has graduated from Mapúa University with the degrees of Bachelor and Master of Science in Mechanical Engineering, in 2015, and 2018, respectively.
He is currently a Senior Science Research Specialist for a CHED – DARE TO research project in the research building of Mapúa University and is also a lecturer for the Mechanical and Manufacturing Engineering department of Mapúa University. He has previously presented his M.S. thesis at the 2018 International Conference on Ocean Energy, held in Cherbourg France, and at the 2018 International Conference on Sustainable Environmental Technologies in Manila. His research interests include marine renewable energy, drone technology, tidal energy resource assessment, and numerical simulation.
He has won the First Place in the Poster Awards of the 2018 International Conference on Ocean Energy, out of 69 accepted posters and has been recognized and acknowledged for this achievement by Mapúa University and by the Governor of Batangas, his home province.

Mark Christian E. Manual was a PhD graduate of the Chung Yuan Christian University in Taiwan.
He is currently the Dean of the School of Mechanical and Manufacturing Engineering of Mapúa University. He has published numerous journal articles, some of which are: "Optimal duct layout for HVAC using topology optimization", "A Survey of Indoor Environmental Quality Studies in the Philippines from 2003 to 2017", and "Development of a Laboratory Set-Up of a Horizontal Slinky-Loop Ground-Coupled Air-Conditioning System". His research interests include design optimization theories, topology optimization, thermofluidics, and built environment.

John Marvil R. Chua, Eldric Marius A. Sangalang, and Patrick C. So are undergraduate students of Bachelor of Science in Mechanical Engineering in Mapúa University.
The research interests include instrumentations, robotics, and rapid prototyping.